ANALYSIS OF EXTERNAL HEAT DISSIPATION ENHANCEMENT OF OIL-IMMERSED TRANSFORMER BASED ON FALLING FILM MEASURE

by

Yingguang LI[a,b], Zeru ZHOU[b], Biren LIN[a*], Hao ZHANG[a], Weifeng HUO[b], Honglei DENG[a], and Gang LIU[a*]

[a] School of Electric Power Engineering, South China University of Technology, Guangzhou, China
[b] Dongguan Power Supply Bureau of Guangdong Power Grid Corporation, Guangdong Dongguan, China

Original scientific paper
https://doi.org/10.2298/TSCI211015041L

With the increase of power load, the overheating problem of oil-immersed transformer in operation cannot be ignored. Therefore, it is necessary to propose reasonable heat dissipation enhancement measure for oil-immersed transformer in operation and study the influence of the measure on the internal temperature of transformer. The heat transfer process of oil-immersed transformer is analyzed, and the air-side heat transfer coefficient is pointed out to be the important parameter limiting the heat dissipation capacity of the transformer. In order to improve heat dissipation capacity, the measures based on cooling fans and falling film are proposed and the calculation methods for the air-side heat transfer coefficient are conducted, respectively. Moreover, the top-oil temperature and hot-spot temperature under two measures are compared by the thermal-fluid coupling model of oil-immersed transformer. For the transformer operating at rated load and the ambient temperature of 25 °C, after the cooling fans are adopted, the top-oil temperature and hot-spot temperature can be reduced by 22.4 °C and 20.7 °C, while after the falling film is adopted, the top-oil temperature and hot-spot temperature can be reduced by 31.2 °C and 28.7 °C, respectively. The results show that the falling film is a more effective heat dissipation enhancement measure, which can meet the higher load demand of oil-immersed transformer.

Key words*: oil-immersed transformer, air-side heat transfer coefficients, heat dissipation enhancement measure, cooling fans, falling film*

Introduction

As a core equipment for power transformation and transmission in the power grid, the operating status of oil-immersed transformers plays an important role in the stable operation of power system [1]. To meet the increasing demand for electrical energy, the capacity of oil-immersed transformer in operation has been increasing, which results in the increase of internal heat generation of transformer. For oil-immersed transformer, the winding hot-spot temperature is the most important limiting factor of transformer load capacity, which should be kept within the specified limits [2, 3]. During the high temperature and high load period, the insufficient heat dissipation of oil-immersed transformer can lead to the excessive hot-spot temperature, which may cause deterioration of the insulation material performance, shorten the service life of the transformer [4, 5]. As a result, it is necessary to take appropriate measures to improve the

* Corresponding authors, e-mail: br1439279630@163.com; liugang@scut.edu.cn

heat dissipation capacity of the oil-immersed transformer, and effectively reduce the internal temperature of the transformer.

To improve heat dissipation efficiency of transformer, some investigations have been carried out. The researches in [6] showed that when ODAN flow was used for cooling, the cooling capacity was enhanced 20.1% over ONAN flow. Then the influence of different oil duct sizes, and the number and position of support blocks on the heat dissipation performance of windings were further discussed in [7-9]. In addition, the researches on optimizing the structure of the panel type radiators were also conducted. In [10], the fin pitch, the fin number of radiators and other structural parameters were optimized to improve the heat dissipation efficiency. Subsequently, to enhance the air disturbance and improve the oil-side heat transfer coefficient, stamping different shapes of vortex generators on the fins was proposed [11]. Moreover, the graphene-doped coating was used to improve the thermal conductivity of radiators with an improvement of 15% [12]. In the aforementioned researches, the proposed heat dissipation enhancement measures provide new thoughts for the production of transformers or panel type radiators. However, for transformers in operation, these measures might not be applicable.

Rodriguez *et al*. in [13] pointed out that the less heat transfer from the outer wall of the radiators to the air is the main reason for limiting the heat dissipation capacity of the radiators. Therefore, some scholars proposed to take external heat dissipation enhancement measures. Currently, the most common measure is to install cooling fans on the radiator. In [14], CFD was used to study the effects of vertical and horizontal air-flow on the oil flow and temperature distribution inside the panel type radiator. Futhermore, the influences of the cooling fans blowing direction and arrangement on the heat dissipation capacity of the panel type radiators were further discussed in [15]. Then, [16] derived the main factors affecting the cooling performance of the radiators and proposed a method of installing cooling fans to achieve efficient cooling. However, when oil-immersed transformers have higher heat dissipation requirements, the economic efficiency of continuing to use cooling fans will be reduced, due to the limit of size and energy consumption of the equipment. Therefore, it is necessary to propose a new measure of panel type radiator for externally enhancing heat dissipation.

In recent years, as a new type of high efficiency heat and mass transfer technique, falling film has been widely used in electronics, refrigeration, and other fields [17]. In this paper, falling film is proposed to improve the heat dissipation capacity of the radiators. Firstly, the heat transfer process of oil-immersed transformer is analyzed in detail and the air-side convective heat transfer coefficient of the radiators is pointed out an important parameter affecting its heat dissipation capacity. Then, the calculation methods of the air-side convective heat transfer coefficient of the radiators under two kinds of external heat dissipation enhancement measures (cooling fans and the falling film) are, respectively conducted. Subsequently, the range of air-side convective heat transfer coefficient under two measures is obtained by simulation model and experiment. Moreover, a 2-D axisymmetric thermal-fluid coupling simulation model of oil-immersed transformer is established to compare and analyze the influence of the two measures on the top-oil temperature and the hot-spot temperature. And the superiority of falling film is also verified. The falling film can effectively reduce the operating temperature of transformer, and it is of great significance for extending the service life of transformer and ensuring the safe operation of the power grid [18].

Analysis of heat transfer process for oil-immersed transformer

When the power transformer is in operation, the heat is generated by the winding, Q_{Cu}, and iron core, Q_{Fe}, transmitted to each surface by heat conduction, and then dissipated

from the surface to the transformer oil by heat convection. Then, the heat of transformer oil is transferred to the oil tank wall and radiator wall by heat convection, and finally the heat on the oil tank wall and radiator wall dissipates to the surrounding environment [19]. A schematic diagram of the heat transfer process of oil-immersed transformer is shown in fig. 1. Where, Q represents the heat dissipating from the oil tank wall and radiator wall to the surrounding environment.

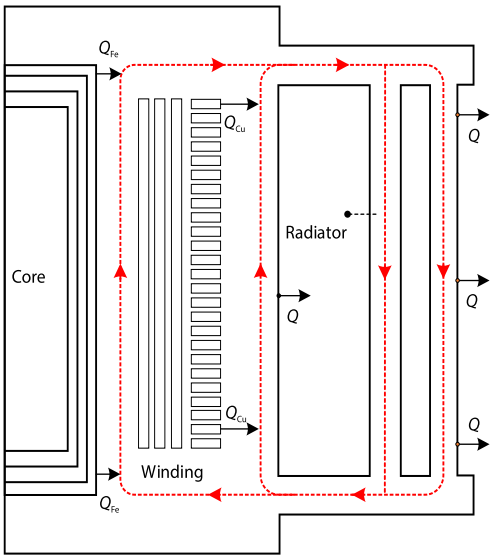

Figure 1. Schematic diagram of heat transfer process of the oil-immersed transformer

According to the aforementioned analysis, the panel type radiator plays a key role in the process of controlling the operating temperature of transformer. In the radiator, the high temperature transformer oil transfers heat to the inner wall of the radiator by heat convection (defined as Process 1). Then, the heat is transferred to the outer wall of the radiator by heat conduction (defined as Process 2). Finally, the heat is dissipated to the surrounding environment by heat convection and heat radiation (defined as Process 3). The three heat transfer processes in the radiator are expressed by the thermal resistance, and the equivalent thermal resistance network is shown in fig. 2.

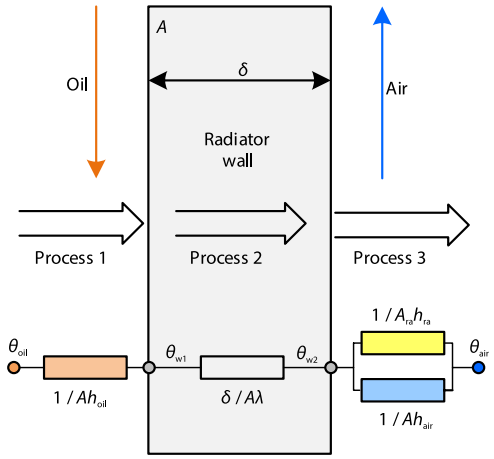

Figure 2. Heat transfer process and equivalent thermal resistance network of panel type radiator

In fig. 2, θ_{oil}, θ_{w1}, θ_{w2} are the temperature of the transformer oil, the inner wall of the radiator and the outer wall of the radiator, respectively, θ_{air} is the ambient temperature, h_{oil} is the oil-side convective heat transfer coefficient of the fin, A is the convective heat transfer area, δ is the thickness of the fin, λ is the thermal conductivity of the fin, h_{air} is the air-side convective heat transfer coefficient of the radiator, h_{ra} is the radiative heat transfer coefficient of the fin, and A_{ra} is the radiation heat transfer area.

Since the thermal conductivity of fin wall with thin thickness is high, the heat conduction thermal resistance $\delta/(A\lambda)$ in Process 2 can be ignored. For Process 3, due to the small spacing between fins, most of the radiative heat between fins is absorbed by the adjacent fins. As a result, the radiative thermal resistance $1/(A_{ra}h_{ra})$ in Process 3 is not considered [20]. When the radiator works in natural-convection, the air-side convective thermal resistance $1/(Ah_{air})$ is about several times to ten times that of its oil-side convective thermal resistance $1/(Ah_{oil})$ [13]. Therefore, the air-side convective thermal resistance is considered as an important parameter that affects the heat dissipation capacity of fins.

In this paper, a 110 kV ONAN transformer with the capacity of 50 MVA, load loss of 179.3 kW and no-load loss of 27.66 kW (hereinafter referred to as the *target transformer*) is taken

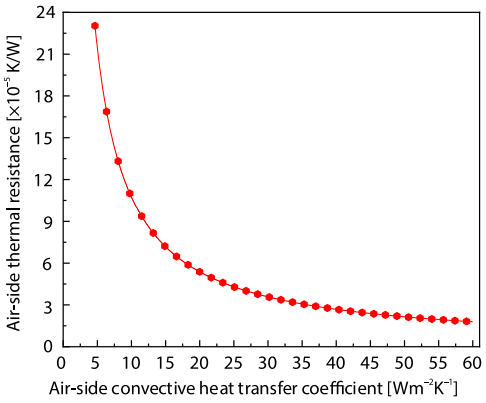

Figure 3. Heat transfer process and equivalent thermal resistance network of panel type radiator

as the object. A total of 14 sets of panel type radiators with the model number PC2500(2000)-21(3)/520 are installed in the target transformer. The convective heat transfer Area A of the panel type radiator can be obtained based on the production data of the target transformer. Then, the air-side convective thermal resistance $1/(Ah_{air})$ of the panel type radiator under different hair are calculated, as shown in fig. 3. It can be seen from fig. 3 that for the case of hair less than 50 W/m^{2}K, as hair increases, the thermal resistance presents an obvious downward trend. However, for the case of hair greater than 50 W/m^{2}K, the decreasing trend of thermal resistance becomes not obvious. Apparently, measures can be taken to increase hair to less than 50 W/m^{2}K, which can effectively reduce the air-side thermal resistance of radiator, and then reduce the operating temperature of oil-immersed transformer.

Combined with the aforementioned analysis, h_{air} is a key parameter for analyzing the heat dissipation capacity of radiator under different enhancement measures. To compare the heat dissipation capacity of radiator, the hot-spot temperature and top-oil temperature under different measures, it is necessary to analyze and calculate the h_{air} according to the heat dissipation mechanism of different measures.

Analysis of heat dissipation performance for panel type radiator with cooling fan installed

Currently, installing cooling fans at the bottom of the radiator is the existing common measure to improve the air-side heat dissipation capacity of the radiator. In this chapter, based on the heat dissipation enhancement mechanism of the cooling fan, a method for obtaining the h_{air} is established. According to the finite element simulation model, the analysis of the enhanced heat dissipation effect of the cooling fan under different operating parameters is realized.

Calculation method of h_{air} of panel type radiator with cooling fan installed

The cooling fans are installed at the bottom of each group of radiators, as shown in fig. 4(a). Considering that the structural dimensions of each group of radiators and the relative positions of the cooling fans are consistent, only one group of them is selected to calculate the h_{air} after installing cooling fans. Figure 4(b) is a cross-sectional view of the panel type radiator at the dotted line in fig. 4(a). In fig. 4(b), due to the size and shape of fan, only some of the fins in a set of radiators, shown in Area A, are affected by fan blowing and in the forced convection state, and the fins that not being blown, shown in Area B, are still in the natural-convection state.

Considering that different fins are in different heat dissipation states, the convective heat transfer coefficient of fins working in natural-convection and forced convection are calculated, respectively. Assuming that there are N_1 fins working in natural-convection and N_2 fins working in forced convection. Then, the average hair can be calculated by eq. (1) to characterize the heat dissipation capacity of the radiator after installing the cooling fan [21]:

$$h_{\text{air}} = \frac{h_{\text{AN}} N_1 + \sum_{i=1}^{N_2} h_{\text{AFavgi}}}{N_1 + N_2} \tag{1}$$

where h_{AN} is the air-side heat transfer coefficient of the fins working in natural-convection and h_{AFavgi} is the air-side convective heat transfer coefficient of the fins working in forced convection.

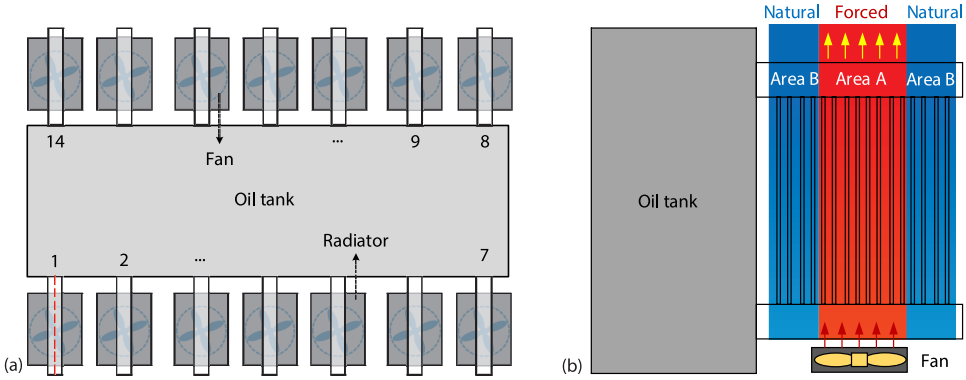

Figure 4. Schematic diagram of cooling fan installed on panel type radiator

For the fins working in natural-convection, h_{AN} can be calculated [21]:

$$h_{\text{AN}} = \frac{\text{Nu}_{\text{AN}} \lambda_{\text{air}}}{L}$$

$$\text{Nu}_{\text{AN}} = \left\{ 0.825 + \frac{0.387 \text{Ra}_{\text{air}}^{1/6}}{\left[1 + \left(\frac{0.492}{\text{Pr}_{\text{air}}} \right)^{9/16} \right]} \right\}^2 \tag{2}$$

$$\text{Ra}_{\text{air}} = \text{Pr}_{\text{air}} \text{Gr}_{\text{air}}$$

$$\text{Pr}_{\text{air}} = \frac{\mu_{\text{air}} C_{p,\text{air}}}{\lambda_{\text{air}}}$$

$$\text{Gr}_{\text{air}} = \frac{g \beta_{\text{air}} \left(\theta_{\text{oil,avg}} - \theta_{\text{air,avg}} \right) L^3}{\frac{\mu_{\text{air}}}{\rho_{\text{air}}}}$$

where Nu_{air}, Ra_{air}, Pr_{air}, and Gr_{air} are the Nusselt number, Rayleigh number, Prandtl number, and Glashof number of the air, respectively, L – the height of fin, λ_{air}, μ_{air}, $C_{p,\text{air}}$, ρ_{air}, β_{air} are the thermal conductivity, dynamic viscosity, specific heat capacity, density, and thermal expansion coefficient of the air, respectively, and θ_{oilavg} and θ_{airavg} – the average temperatures of transformer oil and air.

The fin height, L, the average temperature of transformer oil $\theta_{\text{oil,avg}}$, and the average temperature of air $\theta_{\text{air,avg}}$ are obtained from the transformer factory test report. Then, eq. (2) is used to calculate the h_{AN} of the fin under rated load at the ambient temperature of 25 °C, and the result is 4.7 W/m^{2}K.

For the fins working in forced convection, assume that the average air velocity in the gap between fins is v_{air}, then the average Reynolds number $Re_{air,L}$ can be expressed:

$$Re_{air,L} = \frac{\rho_{air} v_{air} L}{\mu_{air}} \tag{3}$$

Therefore, the h_{AFavg} of fins working in forced convection can be calculated [21]:

$$h_{AF,avg} = \frac{Nu_{AF} \lambda_{air}}{L}$$

$$Nu_{AF} = 0.032 \left\{ \frac{Re_{air,L}^{1/2} Pr_{air}^{1/3}}{\left[1 + \left(\frac{0.0468}{Pr_{air}} \right)^{2/3} \right]} \right\}^{1.6} \tag{4}$$

Due to the unevenness of the blown area on each fin, it is difficult to measure the average air velocity in the gap between fins for the transformer in operation. Therefore, a 3-D simulation model of the radiators with cooling fans will be established in this paper, which is used to calculate the average air velocity v_{air} in the gap between fins under different blowing rate.

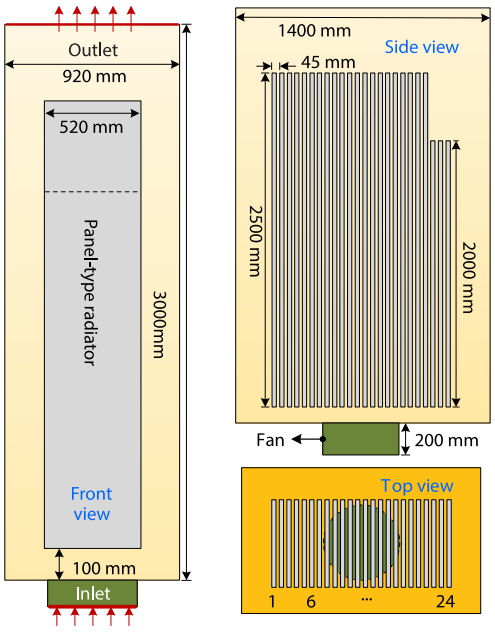

Figure 5. Three views of geometric model of radiator with cooling fan installed

Calculation of h_{air} with cooling fan installed

To study the influence of the impeller diameter and blowing rate of the cooling fan on the heat dissipation enhancement effect, four types of cooling fans are selected. The structure parameters of the two cooling fans are set the diameters are 500 mm and 630 mm, respectively, the fan heights are 200 mm and the cooling fans are 100 mm from the bottom of the radiator. The finite element simulation software is used to build a thermal-fluid coupling simulation model of the radiator with cooling fans installed. The three views of its geometric model are shown in fig. 5. To reduce the amount of calculation, the following simplifications are made in the simulation model [6]:

– ignore the surface shape of fins and simplify it into a rectangular channel and
– ignore the wall thickness of fins.

For the radiator made of carbon steel, its thermal conductivity is set to 54 W/mK [21]. The bottom of the cooling fan is set as the velocity inlet, and the inlet air velocity is set according to the impeller diameter and blowing rate. The inlet air temperature is 25 °C. The top of the air domain is set as a pressure outlet, and the remaining surfaces are set to be non-slip wall. Assume all the heat generated by transformer winding and core at rated load dissipates in convection through the radiator fins, then the heat flux of each fin is given as 213.4 W/m^2.

For the cooling fan with impeller diameter of 500 mm and blowing rate 4200 m^3 per hour, its inlet velocity is set as 5.9 m/s. Then based on the simulation model, the cross-sectional view of the fluid field distribution for each fin gap is obtained as shown in fig. 6. From fig. 6, the air velocity directly above the cooling fan is faster, while the velocity in the gap between the fins on both sides is lower. Furthermore, the average velocity v_{air} of each fin gap under different types of cooling fan are obtained, as shown in fig. 7. It can be found that the average air velocity distribution of the fin gap in Area B in fig. 4(b) is basically not affected by the fan inlet air velocity, while the average air velocity distribution of the fin gap in Area A changes with the change of the inlet air velocity.

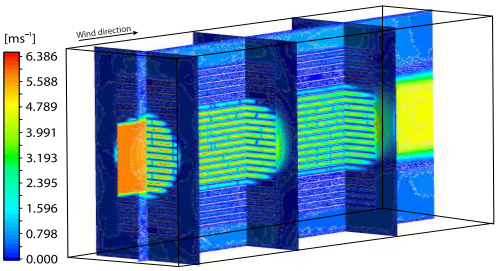

Figure 6. Cross-sectional view of fluid field distribution in the gap between fins

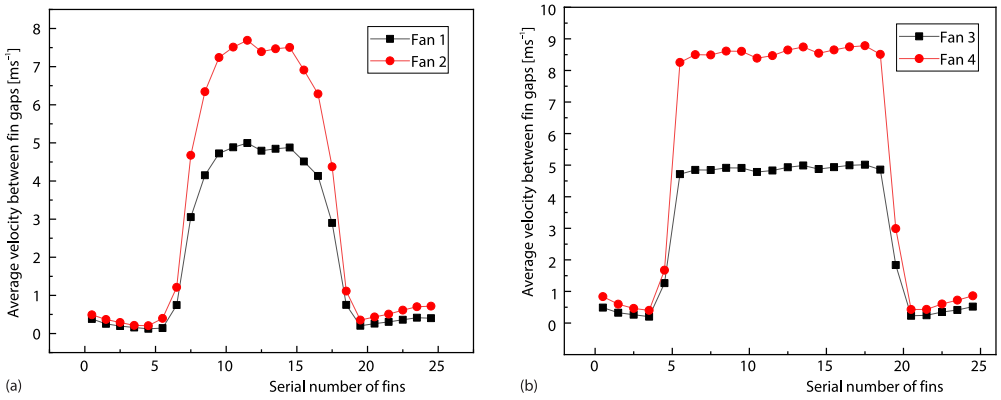

Figure 7. Average air velocity distribution in the gap between fins; (a) impeller diameter is 500 mm and (b) impeller diameter is 630 mm

The $h_{AF,avg}$ of the fin in a forced heat convection state is calculated by eq. (4) using the average air velocity of each fin gap in fig. 7. Combining with eq. (1), hair under different types of cooling fans are calculated, as shown in tab. 1.

Table 1. Average air-side convective heat transfer coefficient of radiator

	Diameter [mm]	Blowing rate [m^{3}h^{-1}]	Inlet velocity [ms^{-1}]	Hair [Wm^{-2}K^{-1}]
Fan 1	500	6400	9.1	11.6
Fan 2	500	4200	5.9	8.7
Fan 3	630	6400	5.7	9.9
Fan 4	630	11000	9.8	14.6

Given from tab. 1, after the cooling fan is installed at the bottom of the radiator, hair is obviously improved. When the impeller diameter is 630 mm and the blowing rate is 11000 m^3 per hour, hair can be increased to 14.6 W/m^{2}K. In combination with fig. 3, the air-side thermal resistance of the panel type radiator still has a certain amount of room to reduce. However, continuing to increase hair needs to increase the impeller diameter or the blowing rate.

Due to the limitation of the size of radiator, it is not applicable to install a cooling fan with larger impeller diameter. On the other hand, increasing the blowing rate of fan will produce more power consumption and increase the fan noise, which brings less economic benefits. Thus, it is necessary to propose a new heat dissipation enhancement measure of to effectively improve hair under the premise of ensuring economy and environmental protection.

Analysis of heat dissipation performance for radiator with falling film measure adopted

According to the aforementioned analysis, when the transformer is required high load operation, the cooling fan hardly meets the heat dissipation demand. Falling film is proposed to reduce the air-side thermal resistance of the radiator and meet the requirements of transformer overload operation.

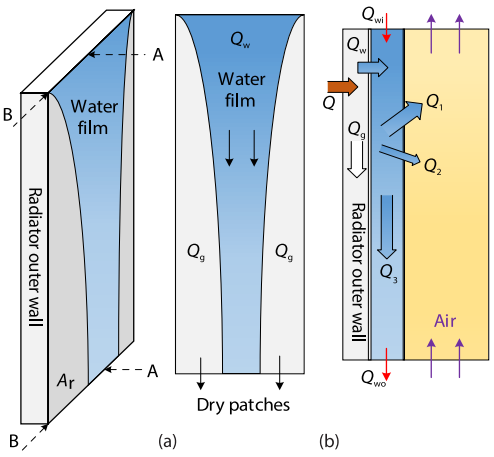

Figure 8. Schematic diagram of heat transfer process of vertical falling film; (a) A-direction view and (b) B-direction view

Heat transfer process of falling film on the vertical wall

The falling film on the vertical wall means that the liquid film flows along the vertical wall under the action of gravity or shearing force. The inner surface of the falling film is attached to the solid surface, and the outer surface is usually in direct contact with outside air or air-flow. Due to the high heat transfer during heat and mass transfer process and the large water film heat transfer coefficient, the falling film has better enhanced heat transfer characteristics [22]. Therefore, it can be used to enhance the external heat dissipation capacity of radiators. In the vertical falling film process, the water flows down along the outer wall of the vertical fins and forms liquid film area and dry patches on the wall. While, the cold air moves from bottom to top and performs heat exchange with the dry patches and the liquid film area. Figure 8 is a schematic diagram of the heat transfer process of vertical falling film. As a result, there is transformer oil flowing through the inner wall of the fins and liquid film flowing through the outer wall, so the heat transfer process of the falling film on the outer wall of the fins can be divided into the following three steps [23]:

- The heat Q is transferred from the transformer oil to the outer wall of fins through the heat conduction of the inner wall of fins.
- If the outer wall of fins is completely covered by the liquid film, the heat is transferred from the outer wall to the liquid film through heat convection. If the liquid film does not completely cover the outer wall, as shown in fig. 8(a), liquid film area and dry patches are formed. Therefore, part of the heat Q_g is dissipated during the convective heat transfer process between the dry patches and the air, and the remaining heat Q_w is transferred to the liquid film through heat convection.
- At the interface between the liquid film and the air, water vapor migrates under the action of the concentration difference, and carries the heat Q_1 to conduct heat and mass transfer with the air in the form of latent heat of vaporization. Meanwhile, part of the heat Q_2 is transferred to the air through heat convection. Finally, because the liquid film is not completely

evaporated, the remaining heat Q_3 is converted into the internal energy of the liquid film to cause the water temperature to change.

Mathematical model of falling film on vertical wall

This paper mainly focuses on the influence of falling film on the air-side heat transfer process of the radiator. The oil-side heat transfer of fins and the wall heat conduction are not considered, and the heat transferred by the oil is simplified to a constant heat Q on the wall. Therefore, according to the previous analysis of the heat transfer process of falling film, the following equation can be obtained:

$$Q = Q_{\mathrm{g}} + Q_{\mathrm{w}} \tag{5}$$

On the assumption that the heat transfer area of the outer wall is A_{r} and the coverage rate of the liquid film is f, then the area of the liquid film is fA_{r} and the area of the dry patches is $A_{\mathrm{r}}(1 - f)$. At the same time, the heat transfer process between dry patches and air can be considered as natural-convection. Therefore, the heat emitted from the dry patches to the air:

$$Q_{\mathrm{g}} = h_{\mathrm{AN}}(1-f)A_{\mathrm{r}}(\theta_{\mathrm{w2}} - \theta_{\mathrm{air}}) \tag{6}$$

Since the air velocity involved in this article is relatively small, it can be considered that the convective heat transfer coefficient between the dry patches and air and between the liquid film and air are both h_{AN} [23].

The heat exchange between the liquid film and the outer wall of fins consists of three parts:

$$Q_{\mathrm{w}} = Q_1 + Q_2 + Q_3 \tag{7}$$

$$\begin{aligned} Q_1 &= h_{\mathrm{m}} f A_{\mathrm{r}} (d_{\mathrm{w}} - d_{\mathrm{air}})\gamma \\ Q_2 &= h_{\mathrm{AN}} f A_{\mathrm{r}} \frac{\theta_{\mathrm{wo}} + \theta_{\mathrm{wi}}}{2 - \theta_{\mathrm{air}}} \\ Q_3 &= C_{p,\mathrm{w}} \dot{m}\left(\theta_{\mathrm{wo}} - \theta_{\mathrm{wi}}\right) \end{aligned} \tag{8}$$

where h_{m} is the mass transfer coefficient, γ – the latent heat of vaporization of water, d_{w} – the moisture content of the air-liquid interface, d_{air} – the air moisture content, θ_{wo} – the outlet water temperature, θ_{wi} – the inlet water temperature, $C_{p,\mathrm{w}}$ – the specific heat capacity of water, and $\dot{m}$ – the mass-flow rate of cooling water.

For the heat and mass transfer process of liquid film and air, the relationship between mass transfer coefficient h_{m} and heat transfer coefficient h_{AN} can be expressed [24]:

$$h_{\mathrm{m}} = \frac{h_{\mathrm{AN}}}{\rho_{\mathrm{air}} C_{p,\mathrm{air}}} \tag{9}$$

The heat transfer process of the outer wall-liquid film-air can be analogized to the convective heat transfer process. Then, the equivalent convective heat transfer coefficient h_{w} between the liquid film and the outer wall can be calculated:

$$h_{\mathrm{m}} = \frac{Q_{\mathrm{w}}}{f A_{\mathrm{r}}\left(\theta_{\mathrm{w2}} - \theta_{\mathrm{air}}\right)} \tag{10}$$

Therefore, the equivalent h_{air} of the outer wall can be calculated:

$$h_{\mathrm{air}} = (1-f)h_{\mathrm{AN}} + f h_{\mathrm{w}} \tag{11}$$

Given from eqs. (5)-(11), if the mass-flow rate of the cooling water, $\dot{m}$, the liquid film coverage rate, f, the ambient temperature, θ_{air}, (the dry and wet bulb temperature), the inlet water temperature, θ_{wi}, and the outlet water temperature, θ_{wo}, are known, h_{air} of fins based on the falling film can be calculated.

Calculation of h_{air} using falling film measure

To evaluate the effect of falling film on the heat dissipation capacity of radiators, a simulation test platform is built to obtain the liquid film coverage rate and other data, then the equivalent hair of the vertical steel plate under different experimental conditions are calculated by eq. (11).

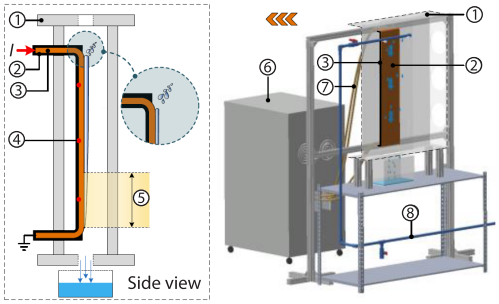

Figure 9. Falling film simulation experiment platform: *1 – plexiglass test table, 2 – thermal insulation cotton, 3 – painted steel plate, 4 – wall temperature measurement point, 5 – imaging area of the infrared thermal imager, 6 – current generator, 7 – wires and cables, and 8 – PVC pipe fittings*

Figure 9 is a schematic diagram of the falling film simulation experiment platform. The simulation experiment platform is composed of four parts: the simulated heat source heating system, the air-flow system, the cooling water supply system, and the data acquisition equipment. The simulated heat source heating system consists of a current generator, wires and cables, and painted steel plates. The painted steel plate is divided into a horizontal section and a vertical experimental section, and the generator and the plate are connected through wires and cables. To ensure that the heat generated by the plate is only dissipated from the outer wall of vertical section, a layer of insulation cotton is attached to the inner wall and the horizontal section of the plate. In addition, considering that it is challenging to select an actual fin to carry out falling film experiments and the heating power is high, the area of the plate is set to 1/9 of the actual fin, but it is ensured that the heat flux of the plate is the same as the heat flux of the actual fin. According to section *Calculation of h_{air} with cooling fan installed*, the current of the generator was adjusted to 279 A to ensure that the heat flux of the plate is 213.36 W/m^2.

The air-flow system is composed of a plexiglass test table. The cooling water supply system is composed of PVC pipe fittings, and the cooling water is transported through the PVC pipe fittings. As a result, it starts to spread the film at the top of the vertical experimental section of the plate, then flew downward the plate. Finally, the remaining water flew into a certain volume water tank.

The data acquisition equipment consisted of thermocouples, a split type of thermometer and hygrometer, and an infrared thermal imager. Three thermocouples were arranged on the inner wall of plate to obtain θ_{w2}. Due to the thin thickness and the good thermal conductivity of the plate, it is considered that the temperature of the inner and outer walls of the plate is the same. In the meantime, thermocouples are arranged at the inlet and outlet of the cooling water to obtain θ_{wi}/θ_{wo}. The dry bulb temperature θ_{air} and wet bulb temperature θ_{wb} of the experimental environment are obtained by the thermometer and hygrometer. Meanwhile, the temperature field distribution on the outer wall of the plate is obtained by an infrared thermal imager, and then the liquid film coverage rate f is obtained by an image processing software. The liquid film mass-flow rate, $\dot{m}$, m is calculated by measuring the volume of cooling water flowing through plate within a certain period.

In this paper, a dimensional analysis of the liquid film mass-flow rate, $\dot{m}$, and other variables is conducted, and it is concluded that $\dot{m}$ was the main factor affecting the liquid film heat transfer. Thus, h_{air} of the plate under the different liquid film mass-flow rate, $\dot{m}$, is mainly focused. The data collected by the simulation experiment platform is input into eqs. (5)-(11) to calculate the equivalent h_{air} of the plate. The results are shown in tab. 2.

Table 2. Air-side heat transfer coefficient of steel plate under different mass-flow rates

$\dot{m}$ [$\cdot 10^{-3}$ kgs^{-1}]	f [%]	θ_{air} [°C]	θ_{wb} [°C]	θ_{wi}/θ_{wo} [°C]	θ_{w2} [°C]	h_{air} [Wm^{-2}K^{-1}]
2.2	5.0	31.9	26.9	31.7/35.0	38.1	38.6
3.7	7.8	31.7	26.3	32.8/34.4	35.8	48.0
5.7	9.6	32.2	26.5	32.4/33.7	36.8	54.3
7.8	9.9	32.3	27.2	32.8/33.7	35.8	67.6
10.5	10.5	34.6	27.4	35.8/36.4	37.4	76.4
15.1	20.9	34.6	27.6	35.1/35.6	36.8	117.5
22.2	14.6	34.4	27.5	35.0/35.3	36.8	94.4

Given from tab. 2, with the increase of $\dot{m}$, hair presents a *first increase and then decrease* trend. This is because the heat taken away by the cooling water increases with the increase of $\dot{m}$ [23]. Also, when $\dot{m}$ increases from $2.2 \cdot 10^{-3}$ kg/s to $15.1 \cdot 10^{-3}$ kg/s, the liquid film coverage rate f increases from 5.0-20.9%. It means that the area covered by the liquid film with good heat transfer effect becomes larger, and the heat transfer area of dry patches with poor heat transfer effect becomes smaller. However, when $\dot{m}$ continues to increase to $22.2 \cdot 10^{-3}$ kg/s, h_{air} appears to decline. This is because, affected by the surface structure of the plate, continuing to increase $\dot{m}$, the liquid film will be hard to continue growing in the width direction and tend to increase in its thickness, resulting in poor heat transfer effect on the film side [23]. At the same time, given from tab. 2 that h_{air} of the plate has been greatly improved after falling film is adopted. When the liquid film mass-flow rate is $5.7 \cdot 10^{-3}$ kg/s, h_{air} of the plate can be increased to 54.3 W/m^{2}K.

Comparison between two heat dissipation enhancement measures

The equivalent h_{air} of the radiator under the two enhancement measures have been obtained in previous researches. In order to compare the reduction degree of the hot-spot temperature and top-oil temperature of target transformer under two enhancement measures, a 2-D axisymmetric thermal-fluid coupling simulation model is established. Based on the results, the reference of enhancement measures for the overload operation of transformer can be provided.

Establishment of simulation model

The geometric structure data of target transformer is shown in tab. 3, and the geometric data of panel type radiator has been described in section. To reduce the calculation of the simulation model, the following assumptions for the target transformer are made [24]:

– Simplify the three-phase windings to single-phase winding for analysis and use a 2-D axisymmetric model for simulation modelling.
– Simplify the transformer yoke and iron core column into a cylinder.
– The structural parts are ignored in the geometric model.

Table 3. Basic data of transformer structure model [mm]

Parameters	Value	Parameters	Value
Core diameter	610	Core window height	1600
Tank length	3777	Tank width	1378
Tank height	2005	Thermal head	646
Inner radius of LV winding	317	Outer radius of LV winding	401
The LV winding height	1345	Inner radius of HV winding	436
Outer radius of HV winding	514	The HV winding height	1344

The physical parameters of transformer oil vary greatly with the change of temperature, which can be regarded as a function of temperature, as shown in tab. 4 [25]. The physical parameters of copper, iron cores, and insulating paper are shown in tab. 5 [26].

Table 4. Physical parameters of transformer oil

Physical characteristics	Temperature expression
Dynamic viscosity [$kgs^{-1}m^{-1}$]	$1.36 \cdot 10^{-6}e^{[2797.3/(\theta_{oil}+273)]}$
Specific heat capacity, C_p [$Jkg^{-1}K^{-1}$]	$1960 + 4.005\theta_{oil}$
Density, ρ [kgm^{-3}]	$887 - 0.659\theta_{oil}$
Thermal conductivity, λ [$Wm^{-1}K^{-1}$]	$0.124 - 1.525 \cdot 10^{-4}\theta_{oil}$

Table 5. Physical parameters of solid materials

Material	ρ [kgm^{-3}]	C_p [$Jkg^{-1}K^{-1}$]	λ [$Wm^{-1}K^{-1}$]
Copper	8933	385	401
Silicon steel	7500	450	44
Insulation paper	930	1340	0.19

In the simulation of target transformer temperature field, the unit volume heat sources are applied to the iron core, LV layer windings, and HV disc windings, respectively according to the relevant parameters provided by the manufacturer. Meanwhile, the fin wall is simplified to a smooth wall. And the change of convective heat transfer coefficient is used to equivalently characterize the heat dissipation capacity of the radiator under different enhancement measures.

Analysis of simulation results

Figure 10 is the temperature field distribution cloud map of the target transformer under the rated load and different hair. In figs. 10(a) and 10(b), the hot-spot temperature both appear at the first disc of the HV winding (marked as θ_{hs1} and θ_{hs2}). For the case of the radiator in natural-convection state (h_{air} = 4.7 W/m^{2}K, the hot-spot temperature and top-oil temperature of target transformer obtained by the simulation model are 106.3 ℃ and 80.6 ℃, respectively, while the manufacturer's software values are 105.0 ℃ and 79.0 ℃, respectively. For the case of the radiators installing 14 sets of cooling fans with impeller diameter of 500 mm and blowing rate of 6400 m^3 per hour (h_{air} = 11.6 W/m^{2}K, the hot-spot temperature and top-oil temperature obtained by the simulation model are 88.6 ℃ and 61.2 ℃, respectively, while the manufacturer's values are 87.0 ℃ and 59.0 ℃, respectively. Compared with the manufacturer's software values, the hot-spot temperature differs by 1.3 ℃ and 1.6 ℃, respectively, and the top-oil temperature differs by 1.6 ℃ and 2.2 ℃, respectively. As a result, the thermal-fluid coupling simulation model built in this paper has a better performance on high calculation accuracy.

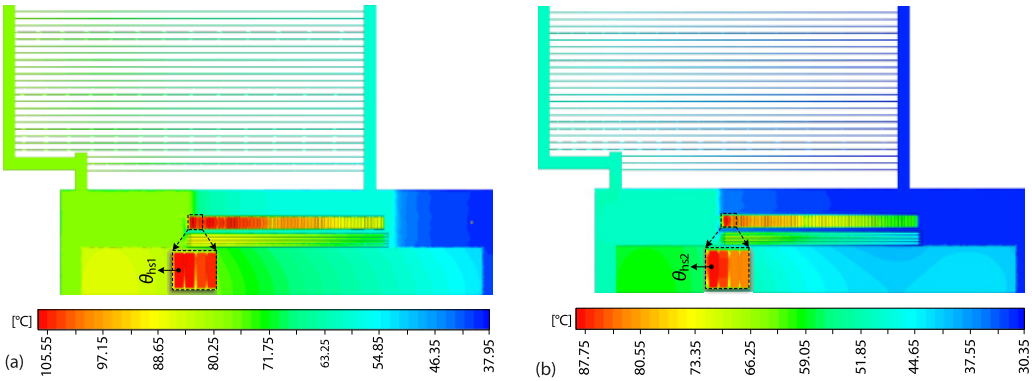

Figure 10. Temperature cloud diagram of target transformer with different h_{air} under rated load; (a) h_{air} = 4.7 W/m²K and (b) h_{air} = 11.6 W/m²K

Comparison of internal temperature of target transformer under different hair

The hot-spot temperature and top-oil temperature of target transformer under different h_{air} can be calculated by the simulation model, and the calculation results are shown in tab. 6.

Table 6. Top-oil temperature and hot-spot temperature under different h_{air}

h_{air} [Wm^{-2}K^{-1}]	Top-oil temperature [°C]	Hot-spot temperature [°C]
4.7	80.6	106.6
11.6	61.2	88.6
14.6	58.2	85.9
20.0	55.0	83.0
30.0	51.9	80.2
40.0	50.4	78.8
50.0	49.4	77.9
60.0	48.8	77.4

Given from tab. 6, if the cooling fans with impeller diameter of 630 mm and blowing rate of 11000 m³ per hour are installed at the bottom of the radiators, compared with natural-convection, the top-oil temperature and hot-spot temperature can be reduced by 22.4 °C and 20.7 °C, respectively. Based on the experimental data in tab. 2, if the falling film is adopted, by adjusting $\dot{m}$, h_{air} can be increased to 50 W/m²K. At this time, the top-oil temperature and hot-spot temperature can be reduced by 31.2 °C and 28.7 °C, respectively. Besides, compared with cooling fans, the falling film can reduce noise and power consumption. Therefore, if the external enhancement heat dissipation measures need to be taken, the falling film measure is more energy-efficient and can bring higher economic benefits.

Conclusions

In this paper, falling film was proposed to improve the heat dissipation capacity of the radiators. The heat transfer process of oil-immersed transformer was analyzed in detail and the air-side convective heat transfer coefficient of the radiators was pointed out an important parameter affecting its heat dissipation capacity. Then, the calculation methods of the air-side

convective heat transfer coefficient of the radiators, h_{air}, under cooling fans and the falling film were, respectively conducted. Subsequently, the range of h_{air} under two measures was obtained by simulation model and experiment. Moreover, a 2-D axisymmetric thermal-fluid coupling simulation model of oil-immersed transformer was established to compare and analyze the influence of the two measures on the top-oil temperature and the hot-spot temperature. The results show that if the cooling fans with impeller diameter of 630 mm and blowing rate of 11000 m^3 per hour are installed at the bottom of the radiators, compared with natural-convection, the top-oil temperature and hot-spot temperature can be reduced by 22.4 ℃ and 20.7 ℃, respectively. While h_{air} of falling film can be increased to 50 W/m^2K by adjusting $\dot{m}$, the top-oil temperature and hot-spot temperature can be reduced by 31.2 ℃ and 28.7 ℃, respectively.

When transformer has high overload requirements, the falling film is a more effective way to strengthen heat dissipation and reduces noise and power loss, which can provide the reference for the selecting enhancement measures for transformers in operation.

Acknowledgment

This research was supported by the Science and Technology Project of Guangdong Power Grid Corporation under Grant No. 031900KK52180153. Support of manufacturing data provided by Siemens Transformer (Guangzhou) Co., Ltd. is gratefully acknowledged.

References

[1] Yigit, C., *et al*., Numerical Investigation of Vapor Phase Drying Process for Drying of Transformer's Insulation Paper, *Thermal Science*, *24* (2020), 3B, pp. 2125-2135
[2] Xu, D. P., *et al.*, Analysis of Winding Temperature Field Under Dynamic Variable Load of Oil-Immersed Transformer, *Thermal Science*, *25* (2021), 4B, pp. 3009-3019
[3] Shiravand, V., *et al*., Improving the Transformer Thermal Modelling by Considering Additional Thermal Points, *International Journal of Electrical Power & Energy Systems*, *128* (2021), 106748
[4] Pierce, L. W., Predicting Liquid Filled Transformer Loading Capability, *IEEE Transactions on Industry Applications*, *30* (1994), 1, pp. 170-178
[5] Susa, D., *et al*., Temperature Rises in an OFAF Transformer at OFAN Cooling Mode in Service, *IEEE Transactions on Power Delivery*, *20* (2005), 4, pp. 2517-2525
[6] Kim, M. G., *et al*., Prediction and Evaluation of the Cooling Performance of Radiators Used in Oil-Filled Power Transformer Applications with Non-direct and Direct-Oil-Forced Flow, *Experimental Thermal and Fluid Science*, *44* (2013), Jan., pp. 392-397
[7] Mufuta, J. M., *et al*., Modelling of the Mixed Convection in the Windings of a Disc-type Power Transformer, *Applied Thermal Engineering*, *20* (2000), 5, pp. 417-437
[8] Taghikhani, M. A., *et al*., Prediction of Hottest Spot Temperature in Power Transformer Windings with Non-directed and Directed Oil-forced Cooling, *International Journal of Electrical Power & Energy Systems*, *31* (2009), 7-8, pp. 356-364
[9] Wu, W., *et al*., Computational Fluid Dynamics Calibration for Network Modelling of Transformer Cooling Oil Flows-Part I Heat Transfer in Oil Ducts, *IET Electric Power Applications*, *6* (2012), 1, pp. 19-27
[10] Liang, Y. M., *et al*., The Optimization of Group Panel-Type Radiator of Transformer, *Applied Mechanics and Materials*, *733* (2015), Feb., pp. 615-18
[11] Garelli, L., *et al*., Heat Transfer Enhancement in Panel Type Radiators Using Delta-wing Vortex Generators, *International Journal of Thermal Science*, *137* (2019), Mar., pp. 64-74
[12] Yin, Z. D., *et al*., Improving Thermal Conductivity of Radiators Using a Graphene-doped Coating, *Surface Engineering*, *37* (2020), 6, pp. 818-821
[13] Rodriguez, G. R., *et al*., Numerical and Experimental Thermo-fluid Dynamic Analysis of a Power Transformer Working in ONAN Mode, *Applied Thermal Engineering*, *112* (2017), Feb., pp. 1271-1280
[14] Paramane, S. B., *et al*., A Coupled Internal-external Flow and Conjugate Heat Transfer Simulations and Experiments on Radiators of a Transformer, *Applied Thermal Engineering*, *103* (2016), June, pp. 961-970
[15] Paramane, S. B., *et al*., The CFD Study on Thermal Performance of Radiators in a Power Transformer: Effect of Blowing Direction and Offset of Fans, *IEEE Transactions on Power Delivery*, *29* (2014), 6, pp. 2596-2604

[16] Kim, Y. J., *et al*., A Numerical Study of the Effect of a Hybrid Cooling System on the Cooling Performance of a Large Power Transformer, *Applied Thermal Engineering*, *136* (2018), May, pp. 275-286
[17] Darabi, J., *et al*., Falling Film and Spray Evaporation Enhancement Using an Applied Electric Field, *Journal of Heat Transfer-Transactions of the ASME*, *122* (2000), 4, pp. 741-748
[18] Sippola, M., *et al.*, Accurate Prediction of High-frequency Power-Transformer Losses and Temperature Rise, *IEEE Transactions on Power Electronics*, *17* (2002), 5, pp. 835-847
[19] Shiravand, V., *et al*., Prediction of Transformer Fault in Cooling System Using Combining Advanced Thermal Model and Thermography, *IET Generation Transmission & Distribution*, *15* (2021), 13, pp. 1972-1983
[20] Ko, T. H., *et al*., Optimal Reynolds Number for the Fully Developed Laminar Forced Convection in a Helical Coiled Tube, *Energy*, *31* (2006), 12, pp. 2142-2152
[21] Garelli, L., *et al*., Reduced Model for the Thermo-Fluid Dynamic Analysis of a Power Transformer Radiator Working in ONAF Mode, *Applied Thermal Engineering*, *124* (2017), Sept., pp. 855-864
[22] Kim, D. S., *et al*., Flow Patterns and Heat and Mass Transfer Coefficients of Low Reynolds Number Falling Film Flows on Vertical Plates: Effects of a Wire Screen and an Additive, *International Journal of Refrigeration-Revue Internationale Du Friod*, *32* (2009), 1, pp. 138-149
[23] Wei, J. Q., *et al*., Measurement of Liquid Film Coverage on Vertical Plates with Hydrophilic and Structured Surface Treatments, *Industrial & Engineering Chemistry Research*, *60* (2021), 9, pp. 3736-3744
[24] El Wakil, N., *et al.*, Numerical Study of Heat Transfer and Fluid-flow in a Power Transformer, *International Journal of Thermal Science*, *45* (2006), 6, pp. 615-626
[25] Skillen, A., *et al*., Numerical Prediction of Local Hot-spot Phenomena in Transformer Windings, *Applied Thermal Engineering*, *36* (2012), Apr., pp. 96-105
[26] Ruan, J. J., *et al*., The HST Calculation of a 10 kV Oil-Immersed Transformer with 3-D Coupled-Field Method, *IET Electric Power Applications*, *14* (2012), 5, pp. 921-928

Paper submitted: October 15, 2021
Paper revised: November 25, 2021
Paper accepted: December 3, 2021